Acta Crystallographica Section C
Crystal Structure Communications
ISSN 0108-2701

A rhodium(III) complex of the linear diborazine $H_3B{\cdot}NMe_2BH_2{\cdot}NMe_2H$: an intermediate in the dehydrocoupling of $H_3B{\cdot}NMe_2H$

Adrian B. Chaplin* and Andrew S. Weller

Department of Inorganic Chemistry, University of Oxford, Oxford OX1 3QR, England
Correspondence e-mail: a.b.chaplin@warwick.ac.uk

Received 16 September 2011
Accepted 19 October 2011
Online 28 October 2011

The solid-state structure of the rhodium complex (dimethylamine–dimethylaminoborane–borane-κ^2H,H')dihydridobis(triisopropylphosphane-κP)rhodium(III) tetrakis[3,5-bis(trifluoromethyl)phenyl]borate, $[RhH_2(C_4H_{18}B_2N_2)(C_9H_{21}P)_2](C_{32}H_{12}BF_{24})$, is reported. The complex contains the linear diborazine $H_3B{\cdot}NMe_2BH_2{\cdot}NMe_2H$, a kinetically important intermediate in the transition-metal-mediated dehydrocoupling of $H_3B{\cdot}NMe_2H$, ultimately affording the dimeric amino-borane $[H_2BNMe_2]_2$. The structure of the title complex contains a distorted octahedral Rh^{III} centre, with mutually *trans* phosphane ligands and *cis* hydride ligands. The diborazine is bound through two Rh—H—B σ-bonds and exhibits a *gauche* conformation with respect to the B—N—B—N backbone.

Comment

The transition-metal-mediated dehydrogenation and dehydrocoupling of amine-boranes (prototypically $H_3B{\cdot}NH_3$) is an area of significant contemporary interest, having relevance to hydrogen storage and the synthesis of new main-group polymeric materials (Staubitz *et al.*, 2010; Alcaraz & Sabo-Etienne, 2010). Despite this interest, details of the intimate mechanisms of these reactions remain scarce. Such details are particularly significant due to the potential to control the kinetics of hydrogen release and the product distributions of the resulting group 13/15 materials (*e.g.* linear oligomeric, cyclic or polymeric materials).

During the course of our work on the dehydrocoupling of amine-boranes using rhodium and iridium bis-phosphane compounds, we have been engaged in the characterization (solution and solid-state) and reactivity of σ-complexes of BN species implicated in the catalytic cycle of this process, or closely related models [(I)–(XIV) in the scheme; Johnson *et al.*, 2011; Stevens *et al.*, 2011; Alcaraz, Chaplin *et al.*, 2010; Chaplin & Weller, 2010; Douglas *et al.*, 2009, 2008]. The formation of related amine- and amino-borane σ-complexes has also been reported using a range of other metal fragments: $\{M(CO)_5\}$ (M = Cr, Mo, W; Shimoi *et al.*, 1999), $\{M(H)_2(carbene)_2\}^+$ (M = Rh, Ir; Tang *et al.*, 2010*a*,*b*) and $\{Ru(H)_2(PCy_3)_2\}$ (Cy is cyclohexyl; Alcaraz, Vendier *et al.*, 2010).

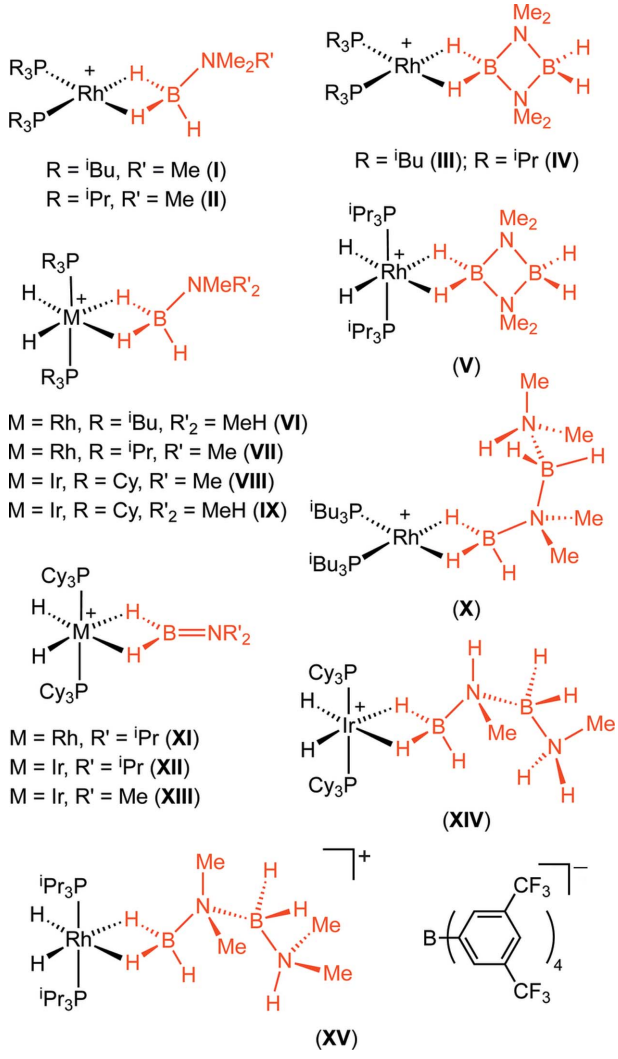

As part of our investigation into the use of $[Rh(PR_3)_2(C_6H_5F)](BAr^F_4)$ [R = ^{i}Pr, ^{i}Bu; Ar^F = $C_6H_3(CF_3)_2$] as catalysts precursor for the dehydrogcoupling of $H_3B{\cdot}NMe_2H$, ultimately affording the dimeric amino-borane $[H_2BNMe_2]_2$, we have demonstrated the kinetic importance of $H_3B{\cdot}NMe_2BH_2{\cdot}NMe_2H$ as an intermediate species (Chaplin & Weller, 2010; Douglas *et al.*, 2009), as have others (Friedrich *et al.*, 2009; Jaska *et al.*, 2003). Due to the high reactivity and dynamic composition of the organometallic species implicated during catalysis, we were only able to characterize a rhodium(I) adduct of $H_3B{\cdot}NMe_2BH_2{\cdot}NMe_2H$ using the $\{Rh(P^iBu_3)_2\}^+$ fragment in the solid state, (X). The structure of a corresponding dihydride rhodium(III) adduct remained elusive, although evidence for such a species had been inferred from solution data (Douglas *et al.*, 2009). We report here the structure of such an adduct, $[Rh(H)_2(\eta^2\text{-}H_3B{\cdot}NMe_2BH_2{\cdot}NMe_2H)(P^iPr_3)_2](BAr^F_4)$, (XV), which crystallized in parallel with $[Rh(H)_2(\eta^2\text{-}H_3B{\cdot}NMe_2H)(P^iPr_3)_2](BAr^F_4)$ during attempted cystallization of the latter, formed from reaction of

 doi:10.1107/S0108270111043447

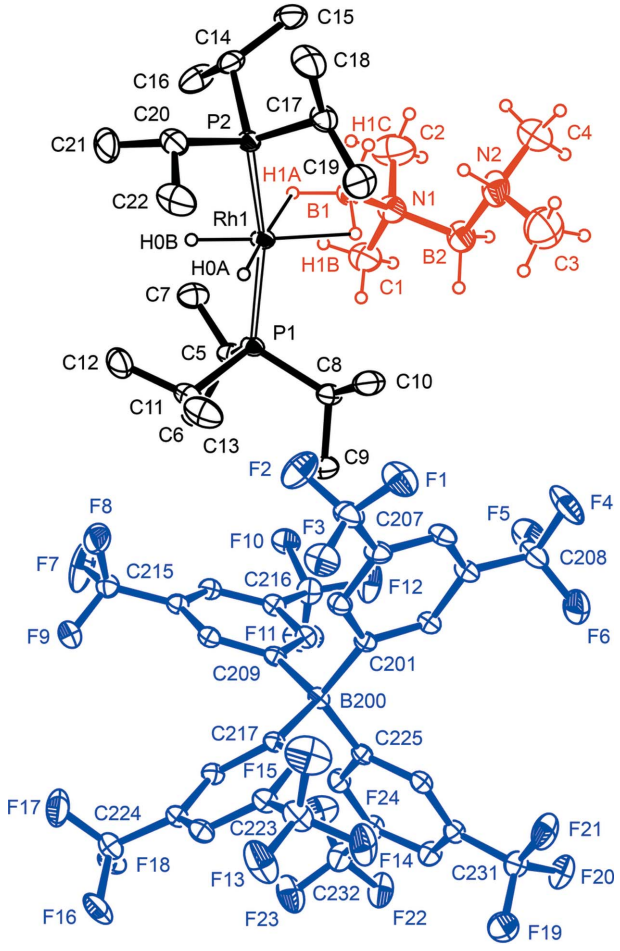

Figure 1
The molecular structure of (XV), showing the atom-numbering scheme. Displacement ellipsoids are drawn at the 30% probability level. Minor disordered components and phosphane H atoms have been omitted for clarity. Selected data are listed in Table 1.

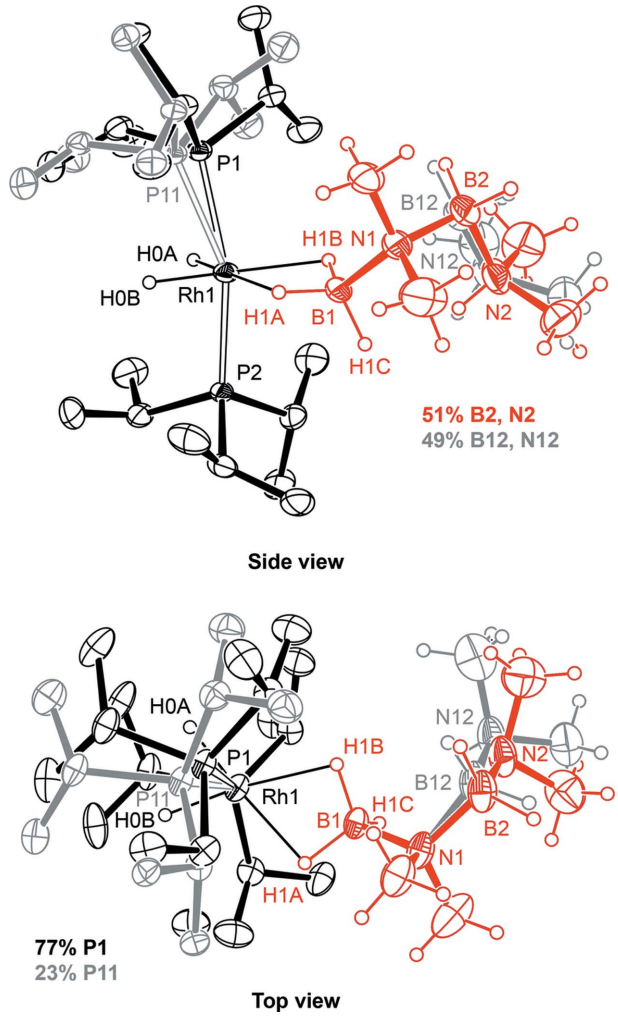

Figure 2
The molecular structure of the cationic portion of (XV), showing the atom-numbering scheme. Displacement ellipsoids are drawn at the 30% probability level. Minor disordered components are shown in light grey. Phosphane H atoms have been omitted for clarity.

$[Rh(P^iPr_3)_2(C_6H_5F)](BAr^F{}_4)$ with two equivalents of $H_3B{\cdot}NMe_2H$. The structure of (XV) is important because it represents a rare example of a highly reactive transition metal B–H σ-complex and, crucially, completes the series of well characterized organometallic intermediates in the dehydrocoupling of amine-boranes (see Scheme), which together add significantly to our understanding of this complex process.

Complex (XV) crystallizes in the triclinic space group $P\overline{1}$; the molecular structure is depicted in Figs. 1 and 2 (cationic portion only), with the atomic numbering schemes. It is best described as having a distorted octahedral Rh^{III} centre with mutually *trans* phosphane ligands and *cis* hydride ligands, a formulation that is fully consistent with the solution NMR characterization. In particular, low-frequency resonances at −0.70 (3H) and −19.6 p.p.m. (2H) in the ^{1}H NMR spectrum confirm the presence of borane and hydride ligands, respectively, in the structure. One of the phosphane ligands is disordered and was consequently modelled over two sites, with the minor component [P11, 0.225 (4)] containing one isopropyl substituent with an inverted conformation to that seen in the major component [P1, 0.775 (4)] (see Fig. 2).

The phosphane ligands are distorted from ideal *trans* geometry, with the P1/P11—Rh1—P2 angles deviating significantly from 180° [160.86 (4) and 153.57 (14)°, respectively] in a similar manner to those observed in the related σ-complexes (V) [151.10 (14)°], (VI) [163.65 (7)°] and (VII) [157.05 (3)°]. The hydride ligands were located in a difference Fourier map and refined to give Rh1—H0*A* and Rh1—H0*B* bond lengths (Table 1) typical of hydride ligands and close to those reported in (V), (VI) and (VII) [1.41 (6)–1.50 (3) Å]. Overall, these metrics are consistent with the $H_3B{\cdot}NMe_2BH_2{\cdot}NMe_2H$ ligand exerting significant steric pressure in the coordination sphere.

The diborazine ligand is partially disordered and was modelled almost equally over two sites from N1 along the B—N—B—N backbone [B2/N2 = 0.511 (14) and B12/N12 = 0.489 (14)]. The components are related to each other by a small torsional twist (Fig. 2). This ligand is bound to the rhodium centre through two Rh—H—B σ-bonds, with Rh1—H1*A* and Rh1—H1*B* distances that are, within error, equivalent (Table 1). The resulting Rh1···B1 distance is 2.316 (4) Å, markedly longer than those in the reported rhodium(I)

analogue (X) [Z' = 2; 2.166 (8) and 2.202 (9) Å]. Such a difference is expected based on the high *trans* influence of the hydride ligands compared with phosphane ligands and has been noted previously for the rhodium(I)–rhodium(III) pairs (II)/(VII) and (IV)/(V). The Rh1···B1 distance is the smallest in the rhodium(III) bis(triisopropylphosphane) σ-complexes (V) [2.386 (15) Å] and (VII) [2.325 (4) Å]. Compared with (XV), the diborazine (albeit the less substituted H_3B··$NMeHBH_2$·$NMeH_2$) in iridium(III) complex (XIV) is more tightly bound, with a shorter Ir···B distance of 2.228 (5) Å.

A notable feature in the structure of (XV) is the conformation of the diborazine ligand, which adopts a *gauche* conformation with respect to the B—N—B—N backbone [|B—N—B—N| = 49.2 (9) and 45.1 (10)° for the major and minor components, respectively]. In rhodium(I) complex (X) [Z' = 2; 47.1 (11) and 44.9 (9)°] and in the free state [45.4 (2)°; Nöth & Thomas, 1999], the diborazine also adopts this conformation. In the case of uncoordinated $H_3B{\cdot}NMe_2BH_2$··NMe_2H, strong intermolecular hydrogen bonds between the hydridic B—H and protic N—H H atoms (*ca* 2.3 Å) were cited as important factors in determining its conformation. However, in both (X) and (XV), no such interactions are observed, presumably because strong packing interactions between the cations and anions predominate. Inspection of Fig. 3 reveals a number of moderately close intermolecular interactions (2.8–3.5 Å), which could suggest that crystal packing effects could play some role in the adoption of the *gauche* conformation of the diborazine in this structure. It is interesting to note that, while the less substituted diborazine $H_3B{\cdot}NMeHBH_2{\cdot}NMeH_2$ adopts a *gauche* conformation in (XIV) [60.0 (4)°], in the free state an *anti* conformation is found [175.90 (11)°] (Johnson *et al.*, 2011).

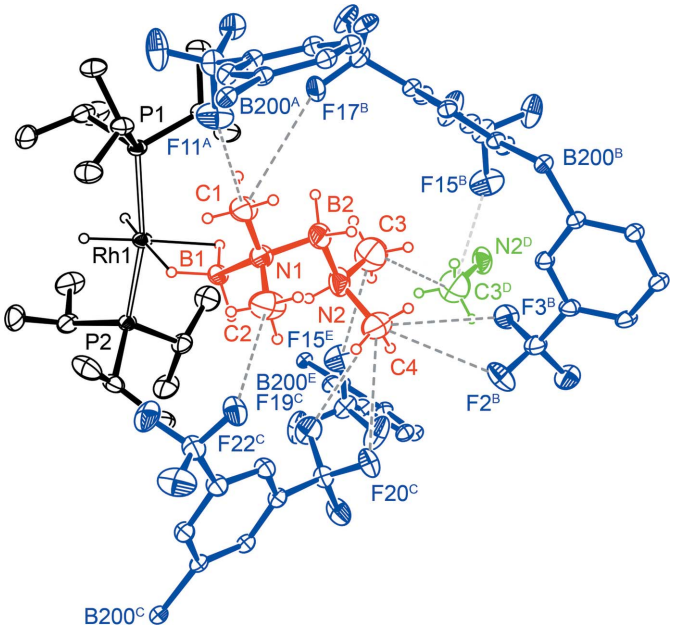

Figure 3
Intermolecular contacts in (XV), with displacement ellipsoids drawn at the 30% probability level. Minor disorder components and phosphane H atoms have been omitted for clarity. Intermolecular interactions between non-H atoms < 3.5 Å are shown with dashed lines. [Symmetry codes: (A) $-x+1, -y+1, -z+1$; (B) $x+1, y, z$; (C) $x+1, y-1, z$; (D) $-x+2, -y+1, -z$; (E) $-x+1, -y+1, -z$.]

Experimental

All manipulations, unless otherwise stated, were performed under an atmosphere of argon, using standard Schlenk and glove-box techniques. Reagents and solvents were prepared and purified as previously described (Chaplin & Weller, 2010). NMR spectra were recorded on a Varian Unity or a Bruker AVC 500 MHz spectrometer.

For the reaction of $[Rh(P^iPr_3)_2(C_6H_5F)](BAr^F_4)$ with $H_3B{\cdot}NMe_2H$, 1,2-$C_6H_4F_2$ (0.4 ml) was added to a J. Young NMR tube charged with $[Rh(P^iPr_3)_2(C_6H_5F)](BAr^F_4)$ (0.010 g, 0.0072 mmol) and $H_3B{\cdot}NMe_2H$ (0.0009 g, 0.015 mmol, 2 equivalents). The reaction was then monitored by NMR spectroscopy, indicating the quantitative formation of the organometallic species $[Rh(H)_2(\eta^2\text{-}H_3B{\cdot}NMe_2H)(P^iPr_3)_2](BAr^F_4)$. Layering the solution with pentane and maintaining the temperature at 278 K (2 d) resulted in the crystallization of a mixture of colourless crystals of $[Rh(H)_2(\eta^2\text{-}H_3B{\cdot}NMe_2H)(P^iPr_3)_2](BAr^F_4)$ and $[Rh(H)_2(\eta_2\text{-}H_3B{\cdot}NMe_2BH_2{\cdot}NMe_2H)(P^iPr_3)_2](BAr^F_4)$ [(XV), ratio 2:1, yield 0.005 g]. Single crystals of the latter were serendipitously picked from solution and placed into the cooling stream on the diffractometer. Spectroscopic data for (XV), ^{1}H NMR (CD_2Cl_2, 500 MHz, 298 K): δ 7.70–7.73 (*m*, 8H, BAr^F_4), 7.56 (*br*, 4H, BAr^F_4), 4.03 (*br*, 1H, NH), 2.68 (*d*, $^3J_{HH}$ = 5.8 Hz, 3H, NH*Me*$_2$), 2.46 (*s*, 3H, NMe_2), 2.15–2.24 (*m*, 6H, PCH), 1.20–1.25 (obscured, 36H, PCMe), −0.70 (vbr obscured, 3H, RhH_3B), −19.6 (apparent *q*, *J* = 17 Hz, 2H, RhH); ^{31}P{^{1}H} NMR (CD_2Cl_2, 202 MHz): δ 64.7 (*d*, $^1J_{RhP}$ = 111 Hz).

Crystal data

$[RhH_2(C_4H_{18}B_2N_2)(C_9H_{21}P)_2](C_{32}H_{12}BF_{24})$
M_r = 1404.43
Triclinic, $P\overline{1}$
a = 12.8309 (2) Å
b = 14.0813 (2) Å
c = 19.1638 (3) Å
α = 73.0175 (6)°
β = 76.4127 (5)°
γ = 86.6877 (6)°
V = 3218.56 (8) Å^3
Z = 2
Mo $K\alpha$ radiation
μ = 0.42 mm^{-1}
T = 150 K
0.22 × 0.10 × 0.10 mm

Data collection

Nonius KappaCCD area-detector diffractometer
Absorption correction: multi-scan (*DENZO/SCALEPACK*; Otwinowski & Minor, 1997)
T_{min} = 0.92, T_{max} = 1.0
24556 measured reflections
14566 independent reflections
11987 reflections with $I > 2\sigma(I)$
R_{int} = 0.018

Refinement

$R[F^2 > 2\sigma(F^2)]$ = 0.047
$wR(F^2)$ = 0.129
S = 1.02
14566 reflections
1069 parameters
1142 restraints
H atoms treated by a mixture of independent and constrained refinement
$\Delta\rho_{max}$ = 0.80 e Å^{-3}
$\Delta\rho_{min}$ = −0.69 e Å^{-3}

The hydride (H0*A* and H0*B*) and BH_3 (H1*A*, H1*B* and H1*C*) H atoms were located in a difference Fourier map and refined as riding, with U_{iso}(H) = 1.2U_{eq}(Rh,B).

The BH_2 H atoms were placed geometrically, with the B—H distance free to refine, using the AFIX 24 instruction (*SHELXL97*; Sheldrick, 2008), and refined as riding, with U_{iso}(H) = 1.2U_{eq}(B). The B—H distance was restrained to equal length across the disorder components (s.u. = 0.001 Å).

Table 1
Selected geometric parameters (Å, °).

Rh1—P1	2.3078 (12)	B1—N1	1.591 (4)
Rh1—B1	2.316 (4)	B1—H1*A*	1.22 (4)
Rh1—P2	2.3259 (7)	B1—H1*B*	1.18 (4)
Rh1—P11	2.397 (5)	B1—H1*C*	1.12 (4)
Rh1—H0*A*	1.44 (3)	N1—B2	1.577 (7)
Rh1—H0*B*	1.44 (3)	N1—B12	1.585 (7)
Rh1—H1*A*	1.88 (4)	B2—N2	1.611 (7)
Rh1—H1*B*	1.91 (4)	B12—N12	1.607 (7)
P1—Rh1—P2	160.86 (4)	H0*A*—Rh1—H0*B*	72.8 (19)
P2—Rh1—P11	153.57 (14)	H1*A*—Rh1—H1*B*	61.1 (16)
B1—N1—B2—N2	−49.2 (9)	B1—N1—B12—N12	−45.1 (10)

The methyl [C—H = 0.98 Å and U_{iso}(H) = 1.5U_{eq}(C)], methenyl [C—H = 1.00 Å and U_{iso}(H) = 1.2U_{eq}(C)], aromatic [C—H = 0.95 Å and U_{iso}(H) = 1.2U_{eq}(C)] and NH [N—H = 0.93 Å and U_{iso}(H) = 1.2U_{eq}(N)] H atoms were placed in calculated positions and refined using the riding model.

Disorder in the structure was treated by modelling the appropriate atom groups independently over two sites, such that the occupancies of the major and minor components summed to unity. Disordered groups included part of the diborazine ligand (B2/N2 and B12/N12), one of the phosphane ligands (P1 and P11) and a number of CF_3 groups of the anion; the F atoms or the entire CF_3 group were modelled over two sites. In each case, the geometries of the components were restrained by allowing bond distances to be the same with a small chemically sensible variation (s.u. = 0.005 Å for N—B and CF_3 C—F bonds; s.u. = 0.01 Å for all other bonds).

Restraints on displacement parameters for atoms within the disordered groups were applied, in order to maintain sensible values for isotropic behaviour (s.u. = 0.007 Å^2) and U^{ij} similarity (s.u. = 0.01 Å^2). The displacement parameters of atoms B2/B12, N2/N12, P1/P11 and C232/C332 were constrained to be identical. Full details of the restraints are given in the archived CIF.

Data collection: *COLLECT* (Nonius, 1998); cell refinement: *DENZO*/*SCALEPACK* (Otwinowski & Minor, 1997); data reduction: *DENZO*/*SCALEPACK*; program(s) used to solve structure: *SIR2004* (Burla *et al.*, 2005); program(s) used to refine structure: *SHELXL97* (Sheldrick, 2008); molecular graphics: *ORTEP-3* (Farrugia, 1997); software used to prepare material for publication: *publCIF* (Westrip, 2010).

The authors thank Dr A. L. Thompson for advice during the preparation of this manuscript. The EPSRC and the University of Oxford are also acknowledged.

Supplementary data for this paper are available from the IUCr electronic archives (Reference: OV3008). Services for accessing these data are described at the back of the journal.

References

Alcaraz, G., Chaplin, A. B., Stevens, C. J., Clot, E., Vendier, L., Weller, A. S. & Sabo-Etienne, S. (2010). *Organometallics*, **29**, 5591–5595.
Alcaraz, G. & Sabo-Etienne, S. (2010). *Angew. Chem. Int. Ed.* **49**, 7170–7179.
Alcaraz, G., Vendier, L., Clot, E. & Sabo-Etienne, S. (2010). *Angew. Chem. Int. Ed.* **49**, 918–920.
Burla, M. C., Caliandro, R., Camalli, M., Carrozzini, B., Cascarano, G. L., De Caro, L., Giacovazzo, C., Polidori, G. & Spagna, R. (2005). *J. Appl. Cryst.* **38**, 381–388.
Chaplin, A. B. & Weller, A. S. (2010). *Inorg. Chem.* **49**, 1111–1121.
Douglas, T. M., Chaplin, A. B. & Weller, A. S. (2008). *J. Am. Chem. Soc.* **130**, 14432–14433.
Douglas, T. M., Chaplin, A. B., Weller, A. S., Yang, X. & Hall, M. B. (2009). *J. Am. Chem. Soc.* **131**, 15440–15456.
Farrugia, L. J. (1997). *J. Appl. Cryst.* **30**, 565.
Friedrich, A., Drees, M. & Schneider, S. (2009). *Chem. Eur. J.* **15**, 10339–10342.
Jaska, C. A., Temple, K., Lough, A. J. & Manners, I. (2003). *J. Am. Chem. Soc.* **125**, 9424–9434.
Johnson, H. C., Robertson, A. P. M., Chaplin, A. B., Sewell, L. J., Thompson, A. L., Haddow, M. F., Manners, I. & Weller, A. S. (2011). *J. Am. Chem. Soc.* **133**, 11076–11079.
Nonius (1998). *COLLECT*. Nonius BV, Delft, The Netherlands.
Nöth, H. & Thomas, S. (1999). *Eur. J. Inorg. Chem.* pp. 1373–1379.
Otwinowski, Z. & Minor, W. (1997). *Methods in Enzymology*, Vol. 276, *Macromolecular Crystallography*, Part A, edited by C. W. Carter Jr & R. M. Sweet, pp. 307–326. New York: Academic Press.
Sheldrick, G. M. (2008). *Acta Cryst.* A**64**, 112–122.
Shimoi, M., Nagai, S.-I., Ichikawa, M., Kawano, Y., Katoh, K., Uruichi, M. & Ogino, H. (1999). *J. Am. Chem. Soc.* **121**, 11704–11712.
Staubitz, A., Robertson, A. P. M., Sloan, M. E. & Manners, I. (2010). *Chem. Rev.* **110**, 4023–4078.
Stevens, C. J., Dallanegra, R., Chaplin, A. B., Weller, A. S., Macgregor, S. A., Ward, B., McKay, D., Alcaraz, G. & Sabo-Etienne, S. (2011). *Chem. Eur. J.* **17**, 3011–3020.
Tang, C. Y., Thompson, A. L. & Aldridge, S. (2010*a*). *Angew. Chem. Int. Ed.* **49**, 921–925.
Tang, C. Y., Thompson, A. L. & Aldridge, S. (2010*b*). *J. Am. Chem. Soc.* **132**, 10578–10591.
Westrip, S. P. (2010). *J. Appl. Cryst.* **43**, 920–925.